Environmental Science and Pollution Research (2024) 31:38385–38398
https://doi.org/10.1007/s11356-024-33759-z

RESEARCH ARTICLE

Dynamic changes in dissolved organic matter during transport of landfill leachate in porous medium

Li Zhao[1,2] · Yucan Lu[1,2] · Jian Yang[3] · Weifang Kong[1,2] · Mingfei Xing[1] · Yiyang Zhang[1]

Received: 11 August 2023 / Accepted: 17 May 2024 / Published online: 28 May 2024

Abstract

The dynamic changes in dissolved organic matter (DOM) during the transport of landfill leachate (LL) in porous medium should be explored, considering the high levels of DOM in the LL of municipal solid waste. Column experiments were carried out at 25 °C at a Darcy's flux of 0.29 cm/h for 2722 h to compare the transport of Cl^-, ultraviolet absorbance at 254 nm (UV_{254}), chemical oxygen demand (COD), and dissolved organic carbon (DOC) in the simulated porous medium by using the CXTFIT2.1 code. Results showed that the convection–dispersion equation (CDE) could describe Cl^- transport well. The high levels of λ and D could be highly correlated with the physicochemical properties of the porous medium. The transport of the studied DOM with evident aromatic character could be described appropriately by the CDE model with the first-order reaction assumption, considering the similar variation trends of UV_{254}, COD, and DOC in the effluent during experiments. Specifically, the values of retardation factor (R) were in the following order: DOC > UV_{254} > COD, whereas the low values of the first-order decay coefficient (k_1) for DOC and COD were still higher than that for UV_{254}. High contents of humic-like substances in the DOM with complex toxic components resulted in the natural low removal efficiencies of COD, DOC, and UV_{254} (≤ 23%), which could be confirmed by the variations of fluorescence index (FI) and humification index (HIX) in the effluent. The results should be helpful in evaluating the environmental risk induced by the LL leakage in a landfill site.

Keywords Municipal solid waste · Leakage of landfill leachate · Silty sand · Transport of dissolved organic matter · Fluorescence · Adsorption

Introduction

According to reports by the "National Bureau of Statistics" of the People's Republic of China, the total amount of municipal solid waste (MSW) in the country has reached approximately 269 Mt in 2021 with a year-on-year growth rate of 5.7% (NBSC 2021; Khan et al. 2022). Thus far, China has produced over 10% of global MSW and has been listed as one of the top three MSW-generating countries in the world (Han et al. 2020; Nanda and Berruti 2021). According to the literature, sanitary landfill accounted for approximately 52% of China's total urban solid waste treatment, whereas incineration and composting accounted for not more that 48% of the total waste in 2018 (Khan et al. 2022). Thus, the sanitary landfill has been the primary technology for the MSW treatment in China in recent decades due to its cost-effectiveness, less labor-intensive procedures, and economic benefits from the utilization of landfill gas (Beaven et al. 2014; Mian et al. 2017; Khan et al. 2022; Nie et al. 2022).

Responsible Editor: Philippe Garrigues

Highlights
- The CDE with first-order reaction assumption explained the DOM transport properly.
- The rates of breakthrough during DOM transport were in the order: COD > UV_{254} > DOC.
- The low values of k_1 for DOC and COD were still slightly higher than that for UV_{254}.
- The humification degree of DOM was enhanced during LL leakage into groundwater.

✉ Jian Yang
JianYang1979@outlook.com

[1] School of Resources and Environment, Henan Polytechnic University, Jiaozuo 454000, China

[2] Shaanxi Key Laboratory of Prevention and Control Technology for Coal Mine Water Hazard, Xi'an 710077, China

[3] College of Geology and Environment, Xi'an University of Science and Technology, Xi'an 710054, China

However, the biodegradation of landfill waste in aerobic environment combined with rainwater percolation through waste as well as the water in the MSW itself produces leachate (Gonçalves et al. 2019). Although the landfill liner layer buried beneath the landfill body could retard the permeation of leachate into underlying aquifers effectively, they eventually deteriorate with time and environmental stress. Moreover, the sharp solid substances in MSW might puncture the impermeable membrane, thereby inducing the leakage of landfill leachate (LL) into the underground environment.

LL is a type of brown solution with foul smell given the complicated components in MSW deposited in landfills (Moravia et al. 2013; Li et al. 2022a, b). It contains a great variety of pollutants including dissolved organic matter (DOM), xenobiotic organic compounds, microorganisms, inorganic macro-components, and heavy metals (Moravia et al. 2013; Jiang et al. 2019; Vaverková et al. 2020). The specific quality of LL is highly correlated with rainfall, climate, waste ingredients, and landfill age. LL with lasting toxicological characteristics usually has extremely high contents of DOM, ammonium nitrogen, and microorganisms, considering that organic fraction (55.9 – 61.2%), plastics and rubber (8.0 – 11.2%), and paper (8.5 – 10.0%) are the largest components of MSW in China and many other countries (Liu et al. 2015; Miao et al. 2019; Ma et al. 2020). In mature LL (more than 10 years old), the concentration of chemical oxygen demand (COD) is commonly less than 4000 mg/L, and the concentration ratio of biochemical oxygen demand (BOD) to COD is usually below 0.1, indicating the low biodegradability of LL (Foo and Hameed 2009). The leakage of LL can result in serious underground water pollution and pose a threat to human health, due to the high levels of organics and ammonia combined with other complex toxic components. Thus, the investigation of LL transport in underground water would be considerably meaningful to estimate the potential environmental contaminant risk and provide theoretical support for the prevention of leakage pollution, waste management, and LL treatment.

DOM as a major component of LL is composed of highly variable compounds, ranging from low-molecular-weight (MW) substances (simple volatile fatty acids) to high-MW compounds, such as aromatic hydrocarbons, humic substances, proteins, phenols, and chlorinated aliphatics (Zhang et al. 2013; Zhu et al. 2013; He and Wu 2015; Li et al. 2022a, b). The interaction with several organic and inorganic pollutants could significantly affect the transport and transformation of various pollutants through adsorption, binding, biochemical reactivity, and aggregation (Jones and Bryan 1998; Leenheer and Croué 2003; Hirose 2007; Qian et al. 2011, 2018; Sun et al. 2013; Ma et al. 2018). In addition, DOM in LL contains hydroxyl, carboxyl, carbonyl, and other active functional groups, which are important carriers for heavy metal migration in soil and groundwater. DOM–metal complexes formed through complexation may completely change the bioavailability and migration of toxic metals in the environment, posing a threat to human and ecological environment (Rikta et al. 2018; Zhang et al. 2020a, b). Thus, high levels of DOM, which usually account for over 85% of the total organic leachate, could significantly affect the quality of water and soil around a landfill site during the transport of LL. The dynamic changes in DOM derived from the leaked LL in ground water and soil should be explored. The findings would be greatly helpful in evaluating the impacts of LL on the surrounding environment of landfill sites and assessing its hazard to human health.

In general, the physicochemical characterization, contaminant hazards, and treatment technology of DOM derived from crude LL have been reported widely (Kang et al. 2002; Zhang et al. 2013; Pan et al. 2017; Jiang et al. 2019; Wang et al. 2020; Ma et al. 2021). Domestic and foreign studies on the migration law of organic matter in groundwater porous media mainly focus on the laboratory simulation of the migration and transformation of certain types of organic matter, such as tetrachloroethylene, aniline, phenol, 2,4-dichlorophenol, polycyclic aromatic hydrocarbons, and organic pesticides. Results show that various factors might affect the migration of organic matter, including media, hydrodynamic conditions, the presence of surfactants and organic solvents, and the concentration of particles and suspended colloids (Cheng et al. 2016; Kadi and Benrachedi 2018; Lan et al. 2018; Zhang et al. 2020a, b; Sun et al. 2021; Li et al. 2022a, b). The combination of laboratory experiments and numerical simulation is a reliable method to evaluate the migration process of organic matter. In the past few decades, the convection–dispersion equation (CDE) with first-order degradation in a homogeneous matrix has been widely used to study the transport of reactive solutes in porous media (Clement et al. 1998; De Wilde et al. 2009; Peyrard et al. 2011; Zhao et al. 2018).

Although Jiang et al. (2019) reported the migration of DOM in LL-contaminated groundwater, less is known about the transport of DOM derived from the leaked LL into groundwater than that of nitrogen, metals, and nonreactive tracers, such as chloride and bromide (Florido et al. 2010; Bero et al. 2016; Zhao et al. 2016, 2018). Moreover, the research on the correlations of ultraviolet absorbance at 254 nm (UV_{254}), dissolved organic carbon (DOC), and COD, which have been widely used to quantify the DOM content, could enrich our understanding of DOM transport during LL leakage. In recent years, the fluorescence-derived indices including fluorescence index (FI), biological/autochthonous index (BIX), and humification index (HIX) could identify the characterization and derivation of DOM effectively (Birdwell and Engel 2010; Zhao et al. 2018). Hence, studying the dynamic changes in DOM (represented by DOC,

COD, and UV_{254}, respectively) during the transport of LL in the porous medium by using fluorescence spectroscopy is a worthwhile endeavor. The study would be meaningful to assess the negative effects of DOM derived from the leaked LL on the surrounding environments of landfill sites scientifically. Accordingly, the findings would be beneficial for MSW management and risk assessment.

The current study aims to (1) investigate the hydrogeological parameters for the transport of solutes in the studied porous medium through column experiments and numerical simulation; (2) explore the dynamic changes in UV_{254}, COD, and DOC and their correlations during the transport of LL in the studied matrix; and (3) quantify the variations of FI, BIX, and HIX in the effluent DOM through the determination of 3D excitation–emission fluorescence during LL transport.

Site description

Focusing on the most common type of landfill, which receives a mixture of municipal and commercial waste (Kjeldsen et al. 2002), the Jiaozuo city MSW sanitary landfill site was selected as the study area. It is located in Zhouliu village (35°9′55″N, 113°26′02″E), Xiuwu County, Jiaozuo city, Henan province, China. The geographical location of the studied sanitary landfill site is shown in Fig. 1. It was constructed using the existing brick kiln pits with a depth between 5 and 8 m below ground level in 2007. It is a plain-type waste landfill surrounded by farmland, with a total area of approximately 369,300 m^2, of which the total landfill reservoir area covers 270,600 m^2. The landfill was officially used in October 2008; it has been 15 years old and becomes an elderly landfill. Thus far, the total amount of landfill waste has amounted to approximately 4.6 million tons, with the maximum landfill height of 30 m above the ground and 12 m below the ground. According to the geotechnical investigation report of the site, the shallow groundwater in the study area is classified as the Quaternary pore aquifer. The groundwater level is 20 – 22 m deep, and the water-bearing matrix is mainly comprised of silty sand.

At present, the amount of LL produced in the landfill area is approximately 170 m^3/days. After being regularly pumped out through the leachate collection and drainage system under the landfill area of waste body, LL is temporarily stored in an adjustment tank with a volume of 33,000 m^3. Thereafter, it is pumped to the sewage treatment system set up in the site for treatment. Under the collection and drainage system of LL, high-density polyethylene (HDPE) film with a thickness of 2 mm and geosynthetic clay liner (GCL) are mainly used for the barrier layer of the landfill reservoir area in the site.

Materials and methods

Column material

The used porous medium is comprised of silty sands obtained from a Quaternary pore aquifer, bared from a 20-m deep pit in the study area. The distribution of grain size was described as follows: 46.9% < 75 μm, 75 μm < 30% < 250 μm, and 23.1% > 250 μm. Prior to use, all samples were air dried, crushed, and ground to pass through a 2-mm screen. According to the X-ray diffraction (XRD) analysis (Bruker, Germany), the mineralogical compositions

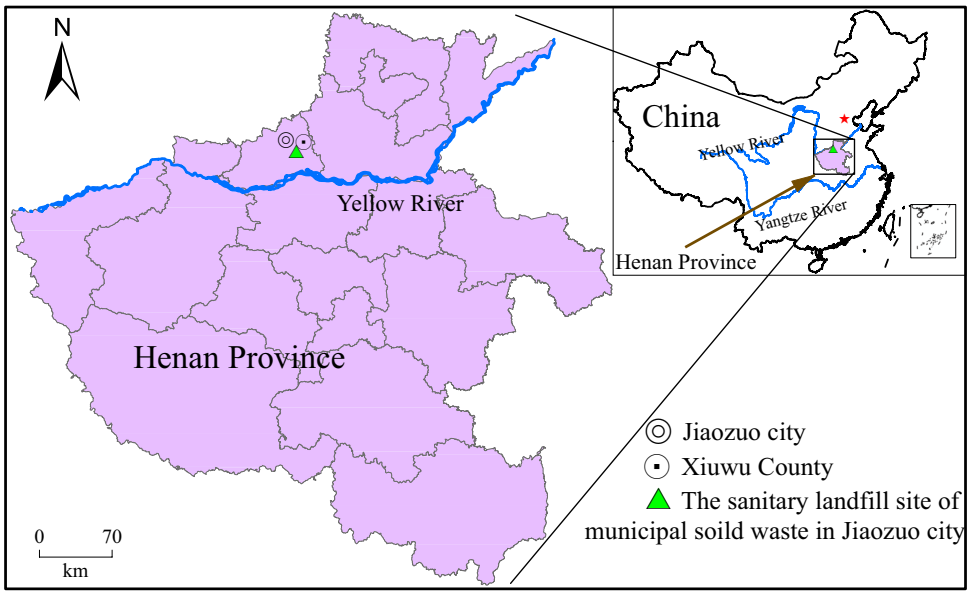

Fig. 1 Location map of the study area

of the sample were quartz (74%), calcite (17%), and feldspar (9%). The total organic carbon (TOC) and cationic-exchange capacity (CEC) were 1.73% and 2.2 cmol/kg, respectively. The soil pH (measured at the ratio of 1:2.5 (*w/v*) silty sand samples to deionized water) was 7.48 using a FG2-FK pH meter (Mettler Toledo Corporation, Switzerland).

Characterization of LL

Approximately, 40 L of LL was sampled from the terminal outlet of the LL collection and drainage system in the landfill reservoir area by using a pump. They were sealed in clean plastic barrels with lids and ring clamps and transported to our laboratory in not more than 2 h. After being filtered through 0.45-μm filter membranes and well-mixed in a clean plastic tank within 24 h, they were stored in a refrigerator at 4 °C before determination. Table 1 shows the physicochemical properties of the collected LL. It was diluted 1/5 with deionized water prior to use for the input solution during column experiments. Thus, the packed silty sand column surface would not be clogged by precipitates induced by the extremely high and complicated contents of pollutants and the decay of microorganisms during the transport of LL through the packed column.

Column design

Figure 2 shows the experimental apparatus used for the column displacement experiments with the diluted LL. Two identical acrylic custom-made columns (11-cm ID and 90-cm height) were packed with the porous medium, as described in the "Column material" section. At the bottom and top inner boundaries of each column, 5-cm thickness of gravel was filled to ensure the water drainage and prevent sand loss. The bottom and top covers of columns were sealed with rubber O-rings to eliminate solution leakage. Two circles of nylon mesh of approximately 11 cm in diameter were individually placed at the bottom and top covers to prevent leaching of silty sand particles. The bulk density and porosity values of the packed matrix in the column were 1.51 g/cm^3 and 0.36 (saturated water content), respectively. The packed columns were placed inside an electrothermal incubator (≤ 85 °C) to maintain the desired temperature. The structure of the electrothermal incubator was described in our previous studies (Zhao et al. 2018).

Initially, deionized water was used to saturate the two vertical columns packed with the porous medium from the bottom using a peristaltic pump (BT100-2 J, Baoding Longer Precision Pump Co., Ltd., China) to expel air in the columns. Thereafter, steady-state rising flow was maintained until the DOC and electrical conductivity (EC) values of the outflow were less than 5 mg/L and 110 μS/cm, respectively. Then, referring to the in situ average Darcy's flux of 0.09 cm/h, the column experiments were carried out here at a Darcy's flux of 0.29 cm/h (hydraulic residence time of 111.8 h) with a test period of 2722 h (23.81 pore volume (PV)) at 25 °C. The PV of the effluents during the elution experiments was calculated by the following:

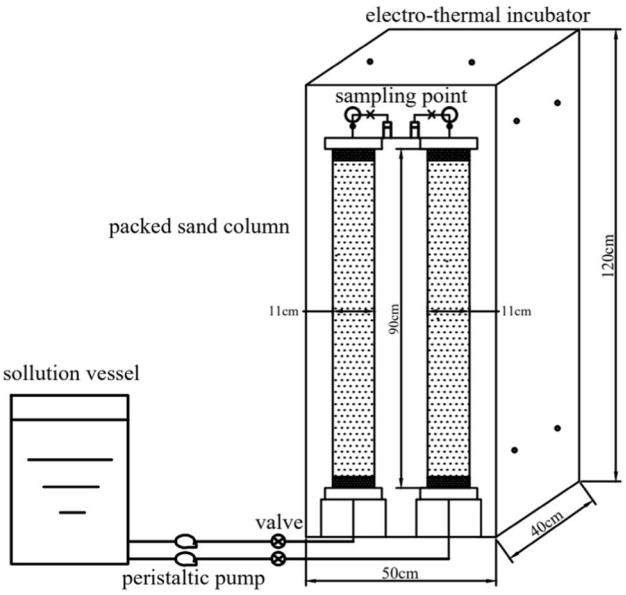

Fig. 2 Schematic drawing of experimental apparatus

$$PV = V_C/V_0 \quad (1)$$

where Vc is the cumulative volume of column effluent (cm^3) and V_0 is the pore volume of the saturated column packed with the studied medium (cm^3).

Sampling and analysis

Samples were collected from the outlet of columns with sampling bottles at pre-set time intervals. The oxidation–reduction potential (ORP) was simultaneously determined for the eluted liquid. After sampling, all samples were

Table 1 Physicochemical properties of the collected LL

COD (mg/L)	DOC (mg/L)	Cl^- (mg/L)	TN (mg/L)	NO_3^--N (mg/L)	Cr^{6+} (mg/L)	Fe^{3+} (mg/L)	UV_{254} (cm^{-1})	EC (μS/cm)	pH
3544.6	1028.5	4870.65	2069.6	19.81	1.41	25.86	24.03	34,227.7	8.18

TN, total nitrogen, mg/L; *EC*, electrical conductivity, μS/cm

filtered through 0.45-μm membranes, stored at 4 °C, and measured for COD, DOC, total nitrogen (TN), UV_{254}, 3D fluorescence spectra, pH, and EC in 24 h. Cl^- in the samples was measured within 7 days.

COD was measured with potassium dichromate method. DOC and total nitrogen (TN) were determined using a TOC-LCSH (Shimadzu Corporation, Japan) with a detector for the TN content. Cl^- was tested through ion-exchange chromatography (ICS-3000, Dionex Co., USA). UV_{254} (cm^{-1}) is expressed as the ratio between optical density at 254 nm and optical length (1.0 cm) using a UV-1800 (Shimadzu Corporation, Japan).

3D excitation–emission fluorescence spectra were acquired in a quartz cell with 1-cm path length by using a fluorescence spectrophotometer (F-7000, Hitachi, Japan). Excitation wavelengths were scanned from 200 to 450 nm, and the emitted fluorescence was detected between 240 and 550 nm in 5-nm steps. The slit width of excitation and emission was 10 nm, and the scan speed was 12,000 nm/min. The Raman peak of water at 348 nm was used to check for instrument stability prior to analysis. FI is the ratio of fluorescence intensities at emission wavelengths of 470 and 520 nm for an excitation at 370 nm (Cory and McKnight 2005). BIX is the ratio of emission intensities at relatively short (380 nm) and long (430 nm) wavelengths at a fixed excitation wavelength (310 nm). HIX is the integrated area under spectra at wavelengths from 435 to 480 nm divided by the sum of the area at wavelengths from 435 to 480 nm and 300 to 345 nm at a fixed excitation wavelength of 254 nm (Ohno 2002).

Deionized water was used for blank samples to make up reagents and clean the quartz cell between samples. All data in this specific study were the average values of the two sequential samples, which had an error of not more than 5%.

Transport model

The convection–dispersion equation (CDE) for 1D transport of reactive solutes (DOC, COD, and UV_{254}) with first-order degradation in a homogeneous medium can be described by the following governing equation:

$$R\frac{\partial C}{\partial t} = -\frac{q}{\theta}\frac{\partial C}{\partial x} + D\frac{\partial^2 C}{\partial x^2} - k_1 C \quad (2)$$

where R is the retardation factor, C (mg/L) is the solute concentration, t (h) is time, q (cm/h) is the Darcy's flux, θ is the porosity (saturated water content), x (cm) is depth, D (cm^2/h) is the hydrodynamic dispersion coefficient, and k_1 (1/h) is the first-order decay coefficient.

The vertical 1D transport of Cl^- in the porous matrix could be described by the CDE model as the following governing equation (Toride et al. 1999; Wang et al. 2013):

$$\frac{\partial C}{\partial t} = -\frac{q}{\theta}\frac{\partial C}{\partial x} + D\frac{\partial^2 C}{\partial x^2} \quad (3)$$

Parameter estimation and data processing

The dynamic changes in Cl^-, COD, DOC, and UV_{254} in the effluent through the matrix were initially determined by analyzing their breakthrough curves (BTCs). Thereafter, the computer software CXTFIT2.1 (Toride et al. 1999) was used to estimate the model parameters of D and pore velocity (υ) based on a nonlinear least-squares fit of the laboratory measurements obtained from the measured BTCs of Cl^- under flux-type boundary conditions. Then, the R and k_1 values for COD, DOC, and UV_{254} were estimated based on their observed BTCs by fixing the simulated values of D and υ for Cl^- using the code. The validity of the first-order reaction assumption for the biodegradation of the studied DOM was investigated by analyzing the numerical results.

Results and discussion

Analysis of Cl^- breakthrough curves

The LL displacement experiments at 25 °C at a Darcy's flux of 0.29 cm/h were carried out. The observed Cl^- BTC was plotted according to the normalized concentrations (C/C_0, hollow symbols) and PV (Fig. 3). As described in the figure, the measured effluent concentrations of Cl^- accounted for more than 98% of the influent value (974.13 mg/L) after 1.8 PV, indicating that the water in the column had been entirely displaced by the injected LL. Thereafter, the measured C/C_0 fluctuated between 0.98 and 1 during the test duration of 23.81 PV (2722 h), suggesting that the reaction of chloride with the packed porous medium and its adsorption onto the matrix could be neglected. Thus, the CDE model was fitted by analyzing the observed BTC to estimate the value of D through CXTFIT 2.1 code.

The simulated BTC for Cl^- is shown in Fig. 3 (solid lines). The fitted results of D and v are presented in Table 2. Despite the complicated components with high contents in the input solution, the CDE model could still describe the vertical transport of Cl^- effectively through the matrix with r^2 and MSE being 0.997 and 0.0005, respectively, as illustrated in the figure and table. The result further confirmed that chloride could be widely used as a conservative tracer in the estimation of solute transport parameters in the porous medium (Broholm et al. 2000; Bero et al. 2016; Eichinger et al. 2020; Shi et al. 2021a). As shown in the table, the value of λ was almost two times that obtained at a Darcy's flux of 0.8 cm/h at 25 °C for the packed fine sand columns (Zhao et al. 2018). Correspondently, the simulated value of D

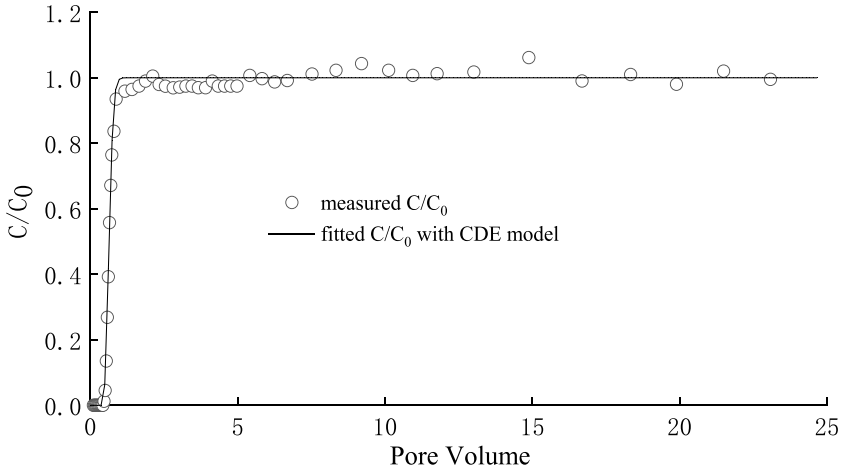

Fig. 3 Observed and fitted BTCs of Cl^- during the transport of LL through the packed silty sand column at a Darcy's flux of 0.29 cm/h at 25 °C (C_0 = 974.13 mg/L). The simulated BTC is presented as —

obtained at the lower Darcy's flux of 0.29 cm/h in this work was close to that reported by Zhao et al. (2018) (D = 1.44 cm^2/h) (Gwo et al. 1995; Toride et al. 2003; Jellali et al. 2010). In addition, the transport of chloride in the studied matrix was dominated by advection, and the role of dispersion for the transport of chloride was evident in the packed column indicated by the low value of Pe (< 100) (Bryant et al. 2003).

Variations in UV_{254}

Figure 4a shows the dynamics of the normalized values (C/C_0) of UV_{254} over PV for the effluent during the elution experiments (hollow symbols). As shown in the figure, the measured values of UV_{254} increased rapidly before 3.24 PV and then tended to be stable. The breakthrough point of UV_{254} was approximately 2 PV later than that of chloride in the effluent, suggesting that the dissolved aromatic compounds might be adsorbed by the packed silty sand containing calcite and feldspar, as described in the "Column material" section (Sø et al. 2012; Al-Anber 2015; Zhang et al. 2018; Xue et al. 2019). Thereafter, the measured values of UV_{254} in the outlet (78–92% of the inlet values) indicated that the removal efficiencies of dissolved aromatic compounds fluctuated between 8 and 22% during LL transport. Thus, a fraction of the DOM could be biodegraded during LL transport in the matrix, as further confirmed by the results obtained in the "Variations in COD and DOC" section.

Assuming that D and q were individually fixed to 1.258 cm^2/h and 0.29 cm/h, respectively, R and k_1 were estimated using CDE model with the first-order degradation assumption (Eq. (2)). The simulated BTC and transport parameters of UV_{254} are shown in Fig. 4a (solid lines) and Table 3, respectively. As shown in the figure, the deviation between the measured and fitting values of C/C_0 for UV_{254} was slightly larger than that of chloride because UV_{254} represents the concentration of a series of compounds with aromatic characters that have ultraviolet absorption at 254 nm instead of one chemical substance (Altmann et al. 2016; Shi et al. 2021b). The special physicochemical properties of these aromatic compounds could induce the slight variations of their transport through the packed matrix, inducing the above result. Nevertheless, the high value of the fitted correlation coefficient (r^2 = 0.95) suggested that the transport of the dissolved aromatic organic matter through the packed sand column could follow the model effectively. The estimated normalized values (C/C_0) of UV_{254} in the outlet were not more than 82% of the inlet values after the breakthrough point. Correspondingly, the simulated values of k_1 and R were 0.00281 h^{-1} and 2.667, respectively, indicating the occurrence of low biodegradation

Table 2 Predicted transport parameters for chloride using CDE model in CXTFIT2.1

T (°C)	q (cm/h)	CDE model				$\lambda(=D/v)$(cm)	$D_h\,(=D\text{-}D_f)$ (cm^2/h)	$Pe\,(=vL/D)$	$D_f\,(=vd/Pe)$ (cm^2/h)
		D (cm^2/h)	v(cm/h)	r^2	MSE				
25	0.29	1.258	1.11	0.997	0.0005	1.14	1.255	79.27	0.003

T temperature, q Darcy's flux, D hydrodynamic dispersion coefficient, v pore-water velocity, L = 90 cm, r^2 correlation coefficient for the regression of observed versus fitted concentration, MSE mean square error, λ dispersivity, D_h mechanical dispersion coefficient, Pe Peclet number, D_f molecular diffusion coefficient, d grain size of the packed silty sand (2 mm)

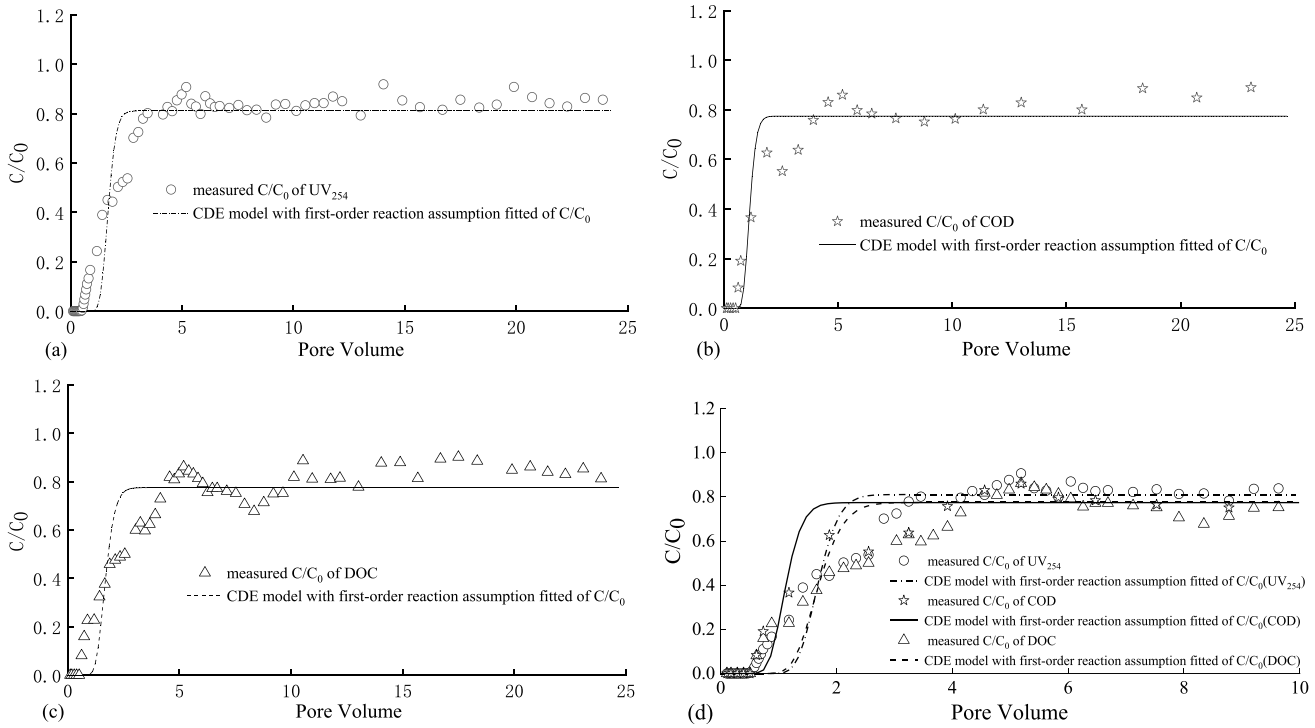

Fig. 4 Observed and fitted BTCs of UV_{254}, COD, and DOC during the transport of LL through the packed silty sand column at a Darcy's flux of 0.29 cm/h at 25 °C

of the aromatic compounds by the packed matrix in the simulated pore groundwater. Calcite and feldspar in the packed porous medium could adsorb the input organic matter as described in literatures (Zhang et al. 2018; Xue et al. 2019). However, the values of R were obviously lower than those obtained in our previous studies due to the lack of clay minerals, such as illite and kaolinite (Zhao et al. 2016, 2019).

Variations in COD and DOC

According to C/C_0 and PV, the observed BTCs of COD and DOC were plotted in Fig. 4 b–c (hollow symbols). In general, the variation trends of COD and DOC were similar to that of UV_{254} in the effluent. Moreover, they could be well expressed as the linear function of UV_{254}, as follows:

$$COD = 129.96UV_{254}, r^2 = 0.97, n = 26 \quad (4)$$

$$DOC = 44.87UV_{254}, r^2 = 0.92, n = 26 \quad (5)$$

where n is the number of measured concentrations in the effluent. The good linear correlation with r^2 is 0.92–0.97 in Eqs. (4) and (5), indicating that UV_{254} could represent the organic content despite its tendency to mainly represent aromatic characters, in accordance with the results of Korshin et al. (2009) and Shi et al.(2021b). In addition, a comparatively strong correlation ($r^2 = 0.94$) is found between the concentrations of COD and DOC, as follows:

$$COD = 2.85DOC, r^2 = 0.94, n = 26 \quad (6)$$

The COD/DOC ratio of 2.85, as shown in Eq. (6), is between 2.84 and 3, as reported in previous studies (Dubber and Gray 2010; Zhao et al. 2020a). The dichromate method (COD_{Cr}), as a measure of chemically oxidizable organics, with more than 2-h test duration, uses heavy metals and produces toxic wastes. By contrast, DOC test, which produces less waste, has the advantage of faster and potentially more precise than COD test. Thus, DOC measured using a high-precision thermocatalytic oxidation

Table 3 Predicted transport parameters for UV_{254}, COD, and DOC using the CDE model in CXTFIT2.1

Parameter	θ	q (cm/h)	CDE model with first-order reaction assumption		
			k_1 (/h)	R	r^2
UV_{254}	0.36	0.29	0.00281	2.667	0.95
COD			0.00353	1.865	0.94
DOC			0.00356	2.792	0.93

θ porosity, q Darcy's flux, k_1 the first-order decay coefficient, R retardation factor, r^2 correlation coefficient for the regression of observed versus fitted concentrations

with a high-temperature TOC analyzer can be used as a potential alternative index of water quality instead of COD to reflect the organic pollution in water (Guo et al. 2017; Park et al. 2022).

As shown in Fig. 4 b–c, the delayed observed BTCs of COD and DOC with the maximum values of not more than 0.9 further confirmed the adsorption and biodegradation of the studied DOM during LL transport through the packed matrix. The simulated BTCs for COD and DOC using the same model as for UV_{254} and the simulated results are shown in Fig. 4b–c (solid lines) and Table 3. The table shows that the high values of r^2 between 0.93 and 0.95 indicate that the CDE model, which has been widely used to investigate the transport of various tracers with curtain structure and chemical composition, could be used to describe the transport of chemically oxidizable organics and DOM with evident aromatic characters. Therefore, chemicals belonging to each surrogate (i.e., COD, DOC, and UV_{254}) in the current work might have similar properties including dispersion, adsorption, and biodegradation.

The differences in the BTCs of UV_{254}, COD, and DOC prior to their breakthrough points could not be distinguished clearly from Fig. 4 a–c, considering the long test duration during the column experiments. Thus, the observed and simulated BTCs of UV_{254}, COD, and DOC were plotted according to the normalized concentrations (C/C_0, hollow symbols) over 10 PV (Fig. 4d). As shown in the figure, the evident delay of the simulated DOC and UV_{254} BTCs compared with that of COD could be observed clearly. In addition, the breakthrough point of UV_{254} was slightly earlier than that of DOC. Correspondingly, the simulated values of R, as shown in Table 3, were in the following order: DOC > UV_{254} > COD. To our best knowledge, DOC represents the total amount of organic carbon present in the measured water samples. By contrast, COD represents both organic and some kinds of reducing inorganic matter that can be oxidized by potassium dichromate, such as Fe^{2+}, NO_2^-, and S^{2-}, which might be adsorbed by the studied porous medium to a less extent than the organic matter in the input LL (Choi et al. 2004; Albrektienė et al. 2012; Zhao et al. 2016, 2018, 2020b). Thus, the rates of breakthrough during DOM transport were in the following order: COD > UV_{254} > DOC. The values of k_1 for DOC and COD were higher than that for UV_{254}, considering the low-molecular-weight aliphatic hydrocarbons were easier to be biodegraded than the aromatic compounds in the DOM during LL transport through the medium. Correspondingly, the simulated maximum values of C/C_0 after the breakthrough points of COD and DOC (0.77–0.78) were slightly lower than that of UV_{254} (0.81). The natural low removal efficiencies of COD, DOC, and UV_{254} could be attributed to the high contents of humic-like substances with low biodegradability (Baker and Curry 2004; Zhang et al. 2013), which could be further confirmed by the results obtained in the "Variations in FI and BIX" and "Variations in HIX" sections.

Variations in FI and BIX

Figure 5a–b shows the variation trends of FI and BIX in the influent and effluent. As illustrated in Fig. 5a–b, the values of FI and BIX in the influent remained stable and fluctuated between 2.98–3.07 and 0.77–0.83, respectively. According to previous studies, DOM might be freshly produced by microbial activities if the calculated FI and BIX values were individually above 1.9 and 0.8, respectively (McKnight et al. 2001; Birdwell and Engel 2010). Thus, abundant microbial precursors were generated during the formation of LL from the landfill waste and their degradation processes, in accordance with the results of Zhang et al. (2013) and Ma et al. (2021).

As shown in Fig. 5a, the FI values in the effluent increased sharply from 2.71 to 4.13 within the initial 0.62 PV. The result could be attributed to the microbe production during the diffusion of the injected solution in the pore water at the beginning of the displacement experiments. However, high contents of DOM, inorganic macro-components, heavy metals, and microorganisms in the input solution would restrain the multiplication and growth of microorganisms when the water in the porous matrix was gradually displaced by the solution (Baker and Curry 2004; Zhang et al. 2013). Thus, the FI values decreased rapidly at PV ranging from 0.62 to 5.42 in the outlet of columns. Thereafter, they stabilized at values between 3.02 and 3.1, which were slightly higher than those in the influent. Hence, the microbes produced during the middle and late stage of column experiments were limited. Low removal efficiencies of COD, DOC, and UV_{254} were observed in the "Variations in COD and DOC" section despite the high values of FI (> 1.9) in the effluent of columns packed with silty sand, considering the low biodegradation characteristics of DOM in LL as reported in previous studies (Baker and Curry 2004; Ma et al. 2021).

Meanwhile, Fig. 5b indicates that the dynamic changes in BIX with PV in the effluent were similar to that of FI due to their similar microbial indications for DOM. Specifically, the calculated values of BIX fluctuated between 1.05 and 1.35 with the average value of 1.21 prior to 0.62 PV, after which it decreased rapidly from 1.2 to 0.74 at PV ranging from 0.62 to 4.15. However, most BIX values in the effluent were still higher than those in the influent at this stage, suggesting that the microbial environment in the simulated pore water strengthened compared with that at the middle and late stage of column experiments (McKnight et al. 2001; Huguet et al. 2009). Thereafter, it tended to be stable at values between 0.79 and 0.81, which was almost equal to the value in the influent. The above phenomenon further confirmed that the amounts of microbes might barely change

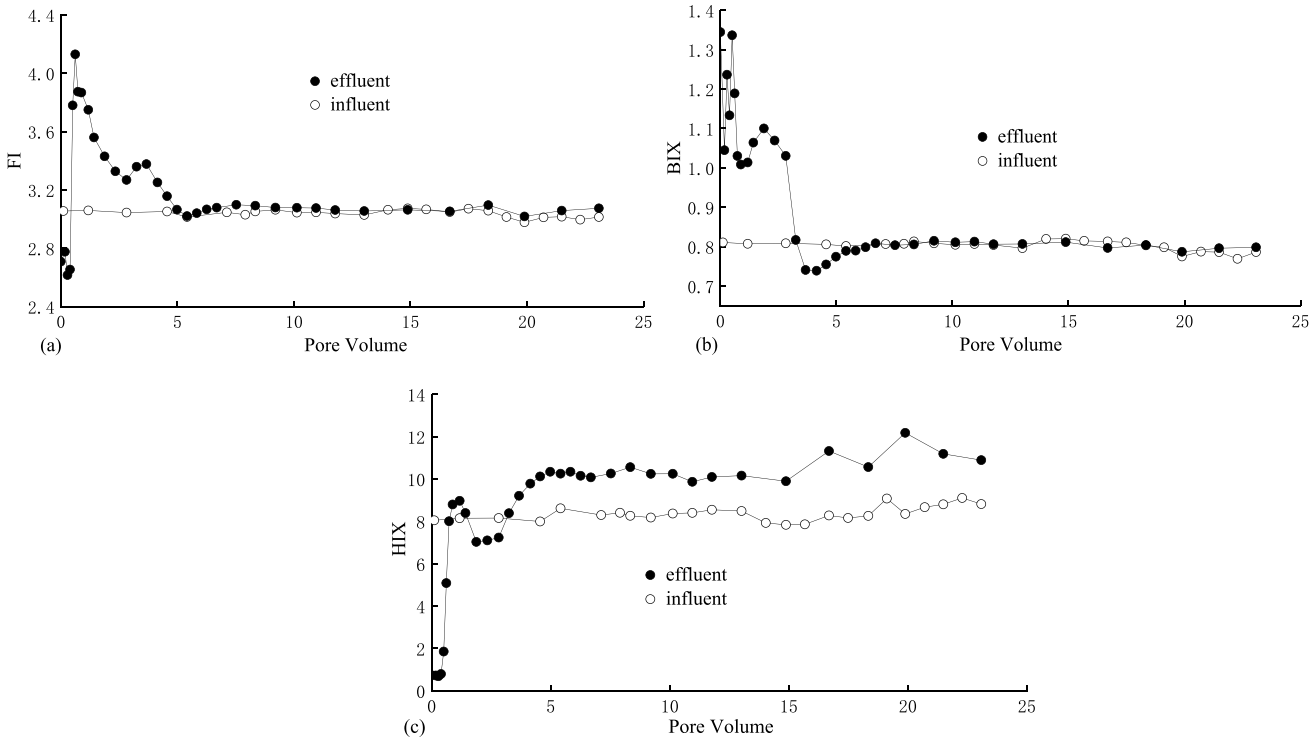

Fig. 5 Variations in FI, BIX, and HIX at 25 °C during column experiments

during the middle and late stage of column experiments, in accordance with the FI results. The types of microbes in the simulated groundwater might change slightly during LL transport due to the biodegradation of a small fraction of the studied DOM.

Variations in HIX

The HIX variations in the influent and effluent during column experiments are shown in Fig. 5c. As shown in the figure, the HIX values in the influent fluctuated between 7.84 and 9.10 due to the heterogeneity of the input LL with high contents of various pollutants. In addition, the long-term test duration with 2722 h could also induce the slight variations of their contents in the collected mature LL maintained at 4 °C in the dark prior to use (the "Characterization of LL" section). DOM, as a major component of LL, is mainly derived from the degradation of plant materials, such as lignin, carbohydrates, and peptides. Thus, it consists of highly variable compounds, such as humic substances, aromatic hydrocarbons, chlorinated aliphatics, and phenols (Jiang et al. 2019; Ma et al. 2021). To our best knowledge, humic substances including humic acid and fulvic acid belong to high-molecular-weight and refractory organic matter, which are difficult to biodegrade (He et al. 2009). They usually account for 39.3–45.4% of the DOC in LL, resulting in high HIX values in the current work (Kang et al. 2002; Zhang et al. 2013; Ma et al. 2021). Therefore, high contents of humic-like substances in the studied DOM with the BIX values lower than 1.0 indicated a strong allochthonous origin of the DOM in the input mature LL (Huguet et al. 2009; Jiang et al. 2019).

As shown in Fig. 5c, the HIX values in the effluent increased sharply from 0.72 to 8.97 within 1.18 PV, after which it decreased within a short period (1.18 ~ 2.82 PV) due to the temporary strengthened microbial environment, as described in the "Variations in FI and BIX" section. Thereafter, the HIX values gradually increased and exceeded the influent values until the end of experiments, implying the enhanced humification degree of the input DOM during the transport of LL through the packed porous medium within the test duration of 2722 h. Moreover, the "exogenous source" characterization of the DOM would be highly correlated with the plant materials derived from MSW (primarily food waste, leaf litter of plants, paper, and wood) and their degradation processes during the leakage of LL in the simulated groundwater beneath the waste body (Yu and Zhang 2016; Tansel 2023).

In summary, the transport of COD, DOC, and UV_{254} in the studied porous medium could be described effectively by the CDE model with the first-order reaction assumption during the leakage of LL into groundwater. However, the adsorption of COD by the packed matrix was the weakest among the three DOM parameters relative to its test method.

During the leakage of LL into groundwater, the composition and content of DOM in LL would be changed due to its weak biodegradability and adsorption onto the porous medium as well as the enhancement of the DOM humification, which could serve as indicators for groundwater pollution. The research in the current work provides a novel scientific perspective for assessing landfill risks and monitoring and remediating groundwater pollution after LL leakage.

ORP, pH, and EC

Variations of ORP, pH, and EC in the outlet of the packed columns over PV are shown in Fig. 6a–c. Figure 6a indicated that the effluent ORP fluctuated between 174 and 297 mV with the injected solution prior to 1.18 PV. Thereafter, it decreased slowly to the minimum value of 105 mV at 23.09 PV, suggesting the strengthening of reducing environment in the simulated pore groundwater with time. Thus, the stable low removal efficiencies of COD, DOC, and UV_{254} were observed. The nitrification of NH_4^+ and reduction in high contents of Fe^{3+} and NO_3^-, as reported in the previous studies (Liu 2019; Miao et al. 2019; Zhao et al. 2020b), could also induce the decrease in ORP in the effluent.

As shown in Fig. 6b, the pH values in the outlet of columns decreased sharply from 8.05 to 6.74 within 3.25 PV. According to the previous studies, ammonium ion is a major nitrogenous compound in LL (Liu 2019; Miao et al. 2019). Its content usually accounts for 58–70% of TN in the liquid. At the beginning of column experiments, aerobic bacteria might be produced during the transport of LL through the packed matrix, indicated by the higher levels of FI and BIX in the effluent than those in the influent. Thus, the high level of ammonium ion would induce the production of the hydrogen ion through weak nitrification reaction under the simulated reduction environment (Huang et al. 2015; Zhao et al. 2016), as follows:

$$NH_4^+ + 2O_2 \rightarrow NO_3^- + 2H^+ + H_2O \quad (7)$$

Moreover, the biodegradation of COD, TOC, and UV_{254} in the current work would induce the production of organic acid with low molecular weight (Liu et al. 2015; Wang et al. 2020). Therefore, a significant decrease in the effluent pH was observed at the beginning of experiments (0–3.25 PV). With the gradual strengthening of reduction environment as well as the complicated and high contents of pollutants in the simulated groundwater, the growth of microorganisms was limited, as described in the "Variations in FI and BIX" section, thereby inducing the inhibition of these reactions. Thus, the rapid increase in effluent pH between 3.25 and 6.04 PV occurred because of the relatively high values of pH in the influent. Thereafter, it tended to be stable at 8.06 ± 0.04, which is still evidently lower than that in the influent. At the middle and late stages of experiments (14.88 ~ 23.88 PV),

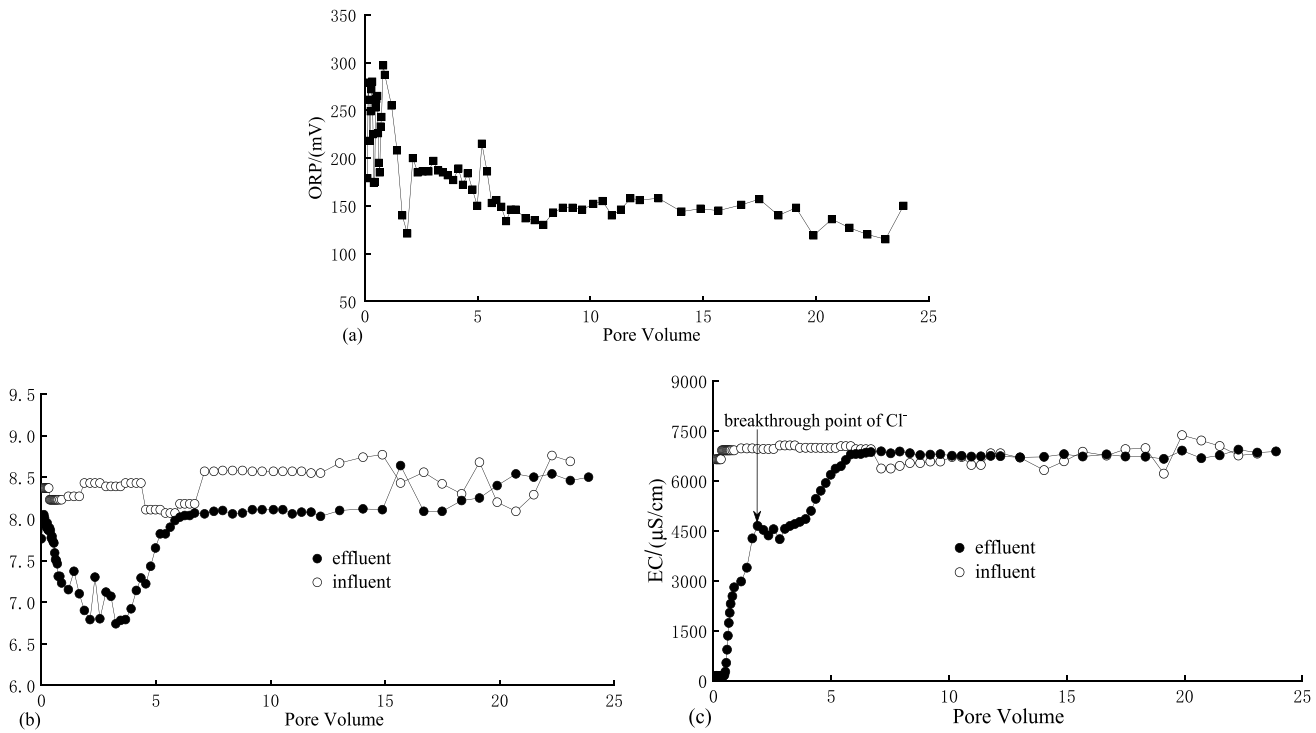

Fig. 6 Variations in ORP, pH, and EC at 25 °C during column experiments

it increased slowly and tended to be stable at the values of the input solution.

Figure 6c showed that the effluent EC increased sharply from 131.5 to 4646 μS/cm prior to 1.88 PV (close to the observed breakthrough point of Cl^-). The transport of sulfate and other ions with low transformation rates and retardation factors through the porous medium might also contribute to the above results (Long et al. 2010; Zhao et al. 2020b). Thereafter, the outlet EC increased rapidly to more than 97% of the input values at 1.88 – 6.05 PV, during which most of the other components would also reach their breakthrough points, such as COD, Fe^{3+}, and Cr^{6+} (not determined here) in the influent (Jung et al. 2006; Ren et al. 2018; Vaverková et al. 2020). Then, the EC values in the effluent stabilized at the influent levels, implying the stabilization of the microbial and physicochemical environments in the studied water.

Conclusion

The BTC of Cl^- at a Darcy's flux of 0.29 cm/h at 25 °C during the transport of mature LL in the studied porous medium could be effectively estimated by the CDE model in the CXTFIT2.1. The values of *Pe*, *D*, and λ suggested that the transport of chloride was dominated by advection in the studied silty sand, and the role of dispersion for its transport was evident. The high levels of D and λ could be highly correlated with the grain size, porosity, and mineralogical compositions of the packed matrix.

The strong linear correlations with r^2 at 0.9–0.97 between values of any two parameters among COD, DOC, and UV_{254} induced their similar variation trends in the effluent during column experiments, thereby suggesting the evident aromatic characteristic of DOM in the studied LL. Their delayed observed BTCs with the maximum values of C/C_0 (≤ 0.92) indicated the occurrence of their low biodegradation and adsorption onto the studied porous medium during LL leakage. Furthermore, the transport of the studied DOM could be described effectively by the CDE model with the first-order reaction assumption in the code. Although chemicals belonging to each surrogate (i.e., COD, DOC, and UV_{254}) might have similar properties including dispersion, adsorption, and biodegradation, the rates of breakthrough were in the following order: COD > UV_{254} > DOC. The k_1 values for DOC and COD were higher than that for UV_{254} because the low-molecular-weight aliphatic hydrocarbons included in COD and DOC were easier to biodegrade than the aromatic compounds indicated by UV_{254} in the DOM.

The high values of HIX in the influent between 7.84 and 9.10 implied the high contents of humic-like substances in the studied mature LL, resulting in the natural low removal efficiencies of COD, DOC, and UV_{254}. These results could be further confirmed by the similar variations of FI, BIX, and ORP in the effluent. Moreover, the humification degree of DOM in the outlet got strengthened during LL transport through the studied porous medium. The variation of pH in the effluent was highly correlated with the biodegradation of DOM and other complicated physical and biochemical interactions during LL transport in the simulated groundwater. Correspondingly, the effluent EC values kept increasing evidently prior to 6.05 PV, after which they stabilized at the input values.

Author contribution All authors contributed to the study conception and design. Material preparation, data collection, and analysis were performed by Li Zhao, Yucan Lu, Jian Yang, Weifang Kong, Mingfei Xing, and Yiyang Zhang. The first draft of the manuscript was written by Li Zhao and Jian Yang, and all authors commented on previous versions of the manuscript. All authors read and approved the final manuscript.

Funding This work was financially supported by the Open Fund Project of Shaanxi Key Laboratory of Prevention and Control Technology for Coal Mine Water Hazard, China (Item No. 2021SKMS04), the National Natural Science Foundation of China (grant no. 52370135), the Doctoral Program Foundation of Henan Polytechnic University (No. B2022-38), and Henan Province Science and Technology Research Key Project for development and promotion in 2024 (Grant No. 242102320079).

Data availability The data that support the findings of this study are openly available on request.

Declarations

Ethical approval The authors declare that they have no known competing financial interests or personal relationships that seem to affect the work reported in this paper. We declare that we have no human participants, human data, or human tissues.

Consent for publication We do not have any person's data in any form.

Conflict of interest The authors declare no competing interests.

References

Al-Anber MA (2015) Adsorption of ferric ions onto natural feldspar: kinetic modeling and adsorption isotherm. Int J Environ Sci Technol 12:139–150

Albrektienė R, Rimeika M, Zalieckienė E, Šaulys V, Zagorskis A (2012) Determination of organic matter by UV absorption in the ground water. J Environ Eng Landsc Manag 20(2):163–167

Altmann J, Massa L, Sperlich A, Gnirss R, Jekel M (2016) UV_{254} absorbance as real-time monitoring and control parameter for micropollutant removal in advanced wastewater treatment with powdered activated carbon. Water Res 94:240–245

Baker A, Curry M (2004) Fluorescence of leachates from three contrasting landfills. Water Res 38(10):2605–2613

Beaven RP, Knox K, Gronow JR, Hjelmar O, Greeddy D, Scharff H (2014) A new economic instrument for financing accelerated landfill aftercare. Waste Manage 34(7):1191–1198

Bero NJ, Ruark MD, Lowery B (2016) Bromide and chloride tracer application to determine sufficiency of plot size and well depth placement to capture preferential flow and solute leaching. Geoderma 262:94–100

Birdwell JE, Engel AS (2010) Characterization of dissolved organic matter in cave and spring waters using UV-Vis absorbance and fluorescence spectroscopy. Org Geochem 41:270–280

Broholm K, Nilsson B, Sidle RC, Arvin E (2000) Transport and biodegradation of creosote compounds in clayey till, a field experiment. J Contam Hydrol 41:239–260

Bryant SL, Paruchuri RK, Saripalli KP (2003) Flow and solute transport around injection wells through a single, growing fracture. Adv Water Resour 26:803–813

Cheng Z, Gao B, Xu HX, Sun YY, Shi XQ, Wu JC (2016) Effects of surface active agents on DNAPL migration and distribution in saturated porous media. Sci Total Environ 571:1147–1154

Choi K, Kim B, Park JH, Kim YH, Jun M (2004) Temporal and vertical variability in the relationship among organic matter indices in a deep reservoir ecosystem. Lake Reservoir Manage 20(2):130–140

Clement TP, Sun Y, Hooker BS, Pertersen JN (1998) Modeling multispecies reactive transport in groundwater aquifers. Ground Water Monit Rem 18(2):79–92

Cory RM, McKnight DM (2005) Fluorescence spectroscopy reveals ubiquitous presence of oxidized and reduced quinones in dissolved organic matter. Environ Sci Technol 39:8142–8149

De Wilde T, Mertens J, Šimunek J, Sniegowksi K, Ryckeboer J, Jaeken P, Springael D, Spanoghe P (2009) Characterizing pesticide sorption and degradation in microscale biopurification systems using column displacement experiments. Environ Pollut 157(2):463–473

Dubber D, Gray NF (2010) Replacement of chemical oxygen demand (COD) with total organic carbon (TOC) for monitoring wastewater treatment performance to minimize disposal of toxic analytical waste. J Environ Sci Health Part A 45(12):1595–1600

Eichinger F, Gimmi T, Möri A, Rüedi J (2020) Profiles of chloride in matrix porewater as natural tracer for matrix diffusion in crystalline rocks. Appl Geochem 118:104635

Florido A, Valderrama C, Arévalo JA, Casas I, Martínez M, Miralles N (2010) Application of two sites non-equilibrium sorption model for the removal of Cu (II) onto grape stalk wastes in a fixed-bed column. Chem Eng J 156(2):298–304

Foo KY, Hameed BH (2009) An overview of landfill leachate treatment via activated carbon adsorption process. J Hazard Mater 171(1–3):54–60

Gonçalves F, Correa CZ, Lopes DD, Vendrame PRS, Teixeira RS (2019) Monitoring of the process of waste landfill leachate diffusion in clay and sandy soil. Environ Monit Assess 191(9):577

Guo W, Yang F, Li YP, Wang SR (2017) New insights into the source of decadal increase in chemical oxygen demand associated with dissolved organic carbon in Dianchi Lake. Sci Total Environ 603:699–708

Gwo JP, Jardine PM, Wilson GV, Yeh GT (1995) A multiple-pore-region concept to modeling mass transfer in subsurface media. J Hydrol 164(1–4):217–237

Han XM, Hu C, Lin L (2020) A study on the impact of China's urbanization on the quantity of municipal solid waste produced. Waste Manage Res 38(2):184–192

He ZQ, Wu FC (2015) Labile organic matter: chemical compositions, function, and significance in soil and the environment. Soil Science Society of America, Madison

He ZQ, Mao JD, Honeycutt CW, Ohno T, Hunt JF, Cade-Menun BJ (2009) Characterization of plant-derived water extractable organic matter by multiple spectroscopic techniques. Biol Fertil Soils 45:609–616

Hirose K (2007) Metal-organic matter interaction: ecological roles of ligands in oceanic DOM. Appl Geochem 22:1636–1645

Huang GX, Liu F, Yang YZ, Deng W, Li SP, Huang YY, Kong XK (2015) Removal of ammonium-nitrogen from groundwater using a fully passive permeable reactive barrier with oxygen-releasing compound and clinoptilolite. J Environ Manage 154:1–7

Huguet A, Vacher L, Relexans S, Saubusse S, Froidefond JM, Parlanti E (2009) Properties of fluorescent dissolved organic matter in the Gironde estuary. Org Geochem 40:706–719

Jellali S, Diamantopoulos E, Kallali H, Bennaceur S, Anane M, Jedidi N (2010) Dynamic sorption of ammonium by sandy soil in fixed bed columns: evaluation of equilibrium and non-equilibrium transport processes. J Environ Manage 91:897–905

Jiang Y, Li R, Yang YN, Yu MD, Xi BD, Li MX, Xu Z, Gao SB, Yang C (2019) Migration and evolution of dissolved organic matter in landfill leachate-contaminated groundwater plume. Resour Conserv Recycl 151:104463

Jones MN, Bryan ND (1998) Colloidal properties of humic substances. Adv Colloid Interface Sci 78(1):1–48

Jung CH, Matsuto T, Tanaka N (2006) Flow analysis of metals in a municipal solid waste management system. Waste Manage 26(12):1337–1348

Kadi N, Benrachedi K (2018) Migration and retention of phenol in three natural soils and effect of solvent. Appl Ecol Environ Res 16(4):4531–4540

Kang KH, Shin HS, Park H (2002) Characterization of humic substances present in landfill leachates with different landfill ages and its implications. Water Res 36(16):4023–4032

Khan S, Anjum R, Raza ST, Bazai NA, Ihtisham M (2022) Technologies for municipal solid waste management: current status, challenges, and future perspectives. Chemosphere 288:132403

Kjeldsen P, Barlaz MA, Rooker AP, Baun A, Ledin A, Christensen TH (2002) Present and long-term composition of MSW landfill leachate: a review. Crit Rev Environ Sci Technol 32(4):297–336

Korshin G, Chow CWK, Fabris R, Drikas M (2009) Absorbance spectroscopy-based examination of effects of coagulation on the reactivity of fractions of natural organic matter with varying apparent molecular weights. Water Res 43:1541–1548

Lan JC, Sun YC, Yuan DX (2018) Transport of polycyclic aromatic hydrocarbons in a highly vulnerable karst underground river system of southwest China. Environ Sci Pollut Res 25:34519–34530

Leenheer JA, Croué JP (2003) Peer reviewed: characterizing aquatic dissolved organic matter. Environ Sci Technol 37(1):18A-26A

Li S, Yang YL, Zheng HS, Zheng YJ, Jing T, Ma J, Nan J, Leong YK, Chang JS (2022a) Advanced oxidation process based on hydroxyl and sulfate radicals to degrade refractory organic pollutants in landfill leachate. Chemosphere 297:134214

Li YH, Bian JM, Wang Q, Li TS (2022b) Experiment and simulation of non-reactive solute transport in porous media. Groundwater 60(3):330–343

Liu ZP, Wu WH, Shi P, Guo JS, Cheng J (2015) Characterization of dissolved organic matter in landfill leachate during the combined treatment process of air stripping, Fenton, SBR and coagulation. Waste Manage 41:111–118

Liu JY (2019) Transport and transformation of ammonia nitrogen during transport of landfill leachate in groundwater. Dissertation, Henan Polytechnic University (in Chinese)

Long YY, Shen DS, Wang HT, Lu WJ (2010) Migration behavior of Cu and Zn in landfill with different operation modes. J Hazard Mater 179(1–3):883–890

Ma J, Guo HM, Lei M, Li YT, Weng LP, Chen YL, Ma YL, Deng YX, Feng XJ, Xiu W (2018) Enhanced transport of ferrihydrite colloid by chain-shaped humic acid colloid in saturated porous media. Sci Total Environ 621:1581–1590

Ma SJ, Zhou CB, Chi C, Liu YJ, Yang G (2020) Estimating physical composition of municipal solid waste in China by applying artificial neural network method. Environ Sci Technol 54(15):9609–9617

Ma Y, Liu ZH, Xi BD, Li WT, Xu YQ, Zhao HZ, Chen ZQ, He XS, Xing BS (2021) Molecular structure and evolution characteristics of dissolved organic matter in groundwater near landfill: implications of the identification of leachate leakage. Sci Total Environ 787:147649

Mcknight DM, Boyer EW, Westerhoff PK, Doran PT, Kulbe T, Andersen DT (2001) Spectrofluorometric characterization of dissolved organic matter for indication of precursor organic material and aromaticity. Limnol Oceanogr 46:38–48

Mian MM, Zeng XL, NasryAal NB, Al-Hamadani SMZF (2017) Municipal solid waste management in China: a comparative analysis. J Materi Cycles Waste Manage 19(3):1127–1135

Miao L, Yang GQ, Tao T, Peng YZ (2019) Recent advances in nitrogen removal from landfill leachate using biological treatments – a review. J Environ Manage 235:178–185

Moravia WG, Amaral MCS, Lange LC (2013) Evaluation of landfill leachate treatment by advanced oxidative process by Fenton's reagent combined with membrane separation system. Waste Manage 33:89–101

Nanda S, Berruti F (2021) Municipal solid waste management and landfilling technologies: a review. Environ Chem Lett 19(2):1433–1456

NBSC (2021) China Statistical Yearbook. National Bureau of Statistics of China. https://data.stats.gov.cn/easyquery.htm?cn¼C01. Accessed 23 July 2022

Nie E, He PJ, Zou JL, Zhang H, Lü F (2022) Neglected effect of transportation on the property of municipal biowaste and the subsequent biomethane potential. J Clean Prod 352:131603

Ohno T (2002) Fluorescence inner-filtering correction for determining the humification index of dissolved organic matter. Environ Sci Technol 36:742–746

Pan HW, Lei HJ, Liu X, Wei HB, Liu SF (2017) Assessment on the leakage hazard of landfill leachate using three-dimensional excitation-emission fluorescence and parallel factor analysis method. Waste Manage 67:214–221

Park JW, Kim SY, Noh JH, Bae YH, Lee JW, Maeng SK (2022) A shift from chemical oxygen demand to total organic carbon for stringent industrial wastewater regulations: utilization of organic matter characteristics. J Environ Manage 305:114412

Peyrard D, Delmotte S, Sauvage S, Namour Ph, Gerino M, Vervier P, Sanchez-Perez JM (2011) Longitudinal transformation of nitrogen and carbon in the hyporheic zone of an N-rich stream: a combined modelling and field study. Phys Chem Earth, Parts a/b/c 36:599–611

Qian JZ, Wang ZP, Jin S, Liu Y, Chen TH, Fallgren PH (2011) Nitrate removal from groundwater in columns packed with reed and rice stalks. Environ Technol 32(14):1589–1595

Qian JZ, Wang XX, Ma L, Wang LP, Liu JK, Yang ZX (2018) Simulation of denitrification in groundwater from Chaohu Lake catchment. China Water Sci Eng 11(2):114–119

Ren X, Liu D, Chen WM, Jiang GB, Wu ZH, Song K (2018) Investigation of the characteristics of concentrated leachate from six municipal solid waste incineration power plants in China. RSC Adv 8(24):13159–13166

Rikta SY, Tareq SM, Uddin MK (2018) Toxic metals (Ni^{2+}, Pb^{2+}, Hg^{2+}) binding affinity of dissolved organic matter (DOM) derived from different ages municipal landfill leachate. Appl Water Sci 8(1):5

Shi PJ, Huang YN, Yang CY, Li Z (2021a) Quantitative estimation of groundwater recharge in the thick loess deposits using multiple environmental tracers and methods. J Hydrol 603:126895

Shi ZN, Chow CWK, Fabris R, Zheng TL, Liu JX, Jin B (2021b) Evaluation of the impact of suspended particles on the UV absorbance at 254 nm (UV_{254}) measurements using a submersible UV-Vis spectrophotometer. Environ Sci Pollut Res 28:12576–12586

Sø HU, Postma D, Jakobsen R, Larsen F (2012) Competitive adsorption of arsenate and phosphate onto calcite; experimental results and modeling with CCM and CD-MUSIC. Geochim Cosmochim Acta 93:1–13

Sun K, Ran Y, Yang Y, Xing BS, Mao JD (2013) Interaction mechanism of benzene and phenanthrene in condensed organic matter: importance of adsorption (nanopore-filling). Geoderma 204–205:68–74

Sun XX, Wang WP, Zhao WD, Qu SS, Zheng QY (2021) Migration characteristics of atrazine in porous media during managed aquifer recharge. Water Supply 21(8):4608–4616

Tansel B (2023) Thermal properties of municipal solid waste components and their relative significance for heat retention, conduction, and thermal diffusion in landfills. J Environ Manage 325:116651

Toride N, Inoue M, Leij FJ (2003) Hydrodynamic dispersion in an unsaturated dune sand. Soil Sci Soc Am J 67:703–712

Toride N, Leij FJ, van Genuchten MTh (1999) The CXTFIT code for estimating transport parameters from laboratory or field tracer experiments. Version 2.1, Research Report 137. US Salinity Laboratory, Riverside, California

Vaverková MD, Elbl J, Koda E, Adamcová D, Bilgin A, Lukas V, Podlasek A, Kintl A, Wdowska M, Brtnický M, Zloch J (2020) Chemical composition and hazardous effects of leachate from the active municipal solid waste landfill surrounded by farmlands. Sustainability 12(11):4531

Wang XY, Zhao L, Liu XM, Lili A, Zhang YX (2013) Temperature effect on the transport of nitrate and ammonium ions in a loose-pore geothermal reservoir. J Geochem Explor 124:59–66

Wang F, Huang YY, Zhuo XC, He C, Li QB (2020) Molecular-level transformation characteristics of refractory organics in landfill leachate during ozonation treatment. Sci Total Environ 749:141558

Xue XP, Wang W, Fan H, Xu ZH, Pedruzzi I, Li P, Yu JG (2019) Adsorption behavior of oxalic acid at water–feldspar interface: experiments and molecular simulation. Adsorption 25:1191–1204

Yu Y, Zhang W (2016) Greenhouse gas emissions from solid waste in Beijing: the rising trend and the mitigation effects by management improvements. Waste Manage Res 34(4):368–377

Zhang QQ, Tian BH, Zhang X, Ghulam A, Fang CR, He R (2013) Investigation on characteristics of leachate and concentrated leachate in three landfill leachate treatment plants. Waste Manage 33(11):2277–2286

Zhang CH, Wei S, Hu YH, Tang HH, Gao JD, Yin ZG, Guan QJ (2018) Selective adsorption of tannic acid on calcite and implications for separation of fluorite minerals. J Colloid Interface Sci 512:55–63

Zhang XY, Su C, Liu XY, Liu ZG, Gu PX, Deng M, Liu Q (2020a) Periodical changes of dissolved organic matter (DOM) properties induced by biochar application and its impact on downward migration of heavy metals under flood conditions. J Clean Prod 275:123787

Zhang YX, Huang XZ, Gao WC, Wang YH, Chang S (2020b) Numerical simulation of chemical reaction–solute transport coupling model of 2,4-DCP in groundwater. Desalin Water Treat 183:346–354

Zhao L, Li YL, Wang SD, Wang XY, Meng HQ, Luo SH (2016) Adsorption and transformation of ammonium ion in a loose-pore geothermal reservoir: batch and column experiments. J Contam Hydrol 192:50–59

Zhao L, Zhao Y, Wang XY, Yang J, Luo SH, Tian YF, Zhen XG (2018) Dynamic changes of dissolved organic matter during nitrate transport in a loose-pore geothermal reservoir. Chem Geol 487:76–85

Zhao L, Sun C, Yan PX, Zhang Q, Wang SD, Luo SH, Mao YX (2019) Dynamic changes of nitrogen and dissolved organic matter during the transport of mine water in a coal mine underground reservoir: column experiments. J Contam Hydrol 223:103473

Zhao L, Du CC, Zhang Q, Sun C, Wang SD, Luo SH (2020a) The ultraviolet–visible absorbance and fluorescence characterization of dissolved organic matter derived from the leaf litter of Populus simonii, Artemisia desertorum, Salix cheilophila, and Populus tomentosa. Environ Sci Pollut Res 27(29):36439–36449

Zhao L, Zhang YY, Wei J, Huang XY, Sun C, Liu JY (2020b) Migration and transformation of iron and chromium from landfill leachate in groundwater. Environ Sci Technol 43(3):74–79 ((**in Chinese**))

Zhu N, Ku TT, Li GK, Sang N (2013) Evaluating biotoxicity variations of landfill leachate as penetrating through the soil column. Waste Manage 33(8):1750–1757